

Understanding the Anthropogenically Forced Change of Equatorial Pacific Trade Winds in Coupled Climate Models*

BAOQIANG XIANG

NOAA/Geophysical Fluid Dynamics Laboratory, Princeton, New Jersey, and University Corporation for Atmospheric Research, Boulder, Colorado, and International Pacific Research Center, University of Hawai'i at Mānoa, Honolulu, Hawaii

BIN WANG

International Pacific Research Center, and Department of Meteorology, University of Hawai'i at Mānoa, Honolulu, Hawaii, and Earth System Modeling Center/NIAMS, Nanjing University of Information Science and Technology, Nanjing, China

JUAN LI

International Pacific Research Center, University of Hawai'i at Mānoa, Honolulu, Hawaii

MING ZHAO

NOAA/Geophysical Fluid Dynamics Laboratory, Princeton, New Jersey, and University Corporation for Atmospheric Research, Boulder, Colorado

JUNE-YI LEE

Institute of Environmental Studies, Pusan National University, Busan, South Korea

(Manuscript received 6 February 2014, in final form 3 August 2014)

ABSTRACT

Understanding the change of equatorial Pacific trade winds is pivotal for understanding the global mean temperature change and the El Niño–Southern Oscillation (ENSO) property change. The weakening of the Walker circulation due to anthropogenic greenhouse gas (GHG) forcing was suggested as one of the most robust phenomena in current climate models by examining zonal sea level pressure gradient over the tropical Pacific. This study explores another component of the Walker circulation change focusing on equatorial Pacific trade wind change. Model sensitivity experiments demonstrate that the direct/fast response due to GHG forcing is to increase the trade winds, especially over the equatorial central-western Pacific (ECWP) (5°S – 5°N , 140°E – 150°W), while the indirect/slow response associated with sea surface temperature (SST) warming weakens the trade winds.

Further, analysis of the results from 19 models in phase 5 of the Coupled Model Intercomparison Project (CMIP5) and the Parallel Ocean Program (POP)–Ocean Atmosphere Sea Ice Soil (OASIS)–ECHAM model (POEM) shows that the projected weakening of the trades is robust only in the equatorial eastern Pacific (EEP) (5°S – 5°N , 150° – 80°W), but highly uncertain over the ECWP with 9 out of 19 CMIP5 models producing intensified trades. The prominent and robust weakening of EEP trades is suggested to be mainly driven by a top-down mechanism: the mean vertical advection of more upper-tropospheric warming downward to generate a cyclonic circulation anomaly in the southeast tropical Pacific. In the ECWP, the large intermodel spread is primarily linked to model diversity in simulating the relative warming of the equatorial Pacific versus the tropical mean sea surface temperature. The possible root causes of the uncertainty for the trade wind change are also discussed.

* School of Ocean and Earth Science and Technology Contribution Number 9186, International Pacific Research Center Contribution Number 1071, and Earth System Modeling Center Publication Number 010.

Corresponding author address: Baoqiang Xiang, NOAA/Geophysical Fluid Dynamics Laboratory, 201 Forrestal Rd., Princeton, NJ 08540.
E-mail: baoqiang.xiang@noaa.gov

1. Introduction

The tropical Pacific is a key region in regulating the earth's weather and climate change on a wide range of time scales. How the tropical Pacific responds to anthropogenic greenhouse gas (GHG) forcing remains an important but highly controversial issue. Regarding the historical data, large discrepancies exist for the twentieth-century sea surface temperature (SST) trend over the tropical Pacific with some data exhibiting an El Niño-like pattern while others showing a La Niña-like pattern (e.g., Vecchi et al. 2008; Deser et al. 2010; Meng et al. 2012; Solomon and Newman 2012; Tokinaga et al. 2012a,b). Similarly, whether the Walker circulation was weakened or intensified over the last century is also a matter of debate (Vecchi et al. 2006; Power and Kociuba 2011; Tokinaga et al. 2012a,b; Meng et al. 2012; L'Heureux et al. 2013). The broad discrepancy in changes of historical SST and circulation pattern in the aforementioned studies is partially due to the paucity of in situ observations over the tropical Pacific, especially over its eastern part. The problem is further complicated by the large multidecadal variability, which can modulate the trend detection.

In contrast to the observed analysis, most state-of-the-art coupled climate models and their multimodel ensemble mean (MME) project an El Niño-like warming under the GHG forcing characterized by more warming in the center and eastern equatorial Pacific than in the western Pacific—that is, reduction of equatorial zonal SST gradients (e.g., Liu et al. 2005; Christensen et al. 2014; Lee and Wang 2014). The resultant greater warming over the equatorial region compared to the subtropics is suggested to be due to the local wind–evaporation–SST feedback (Lu and Zhao 2012) and the relatively weaker mean winds over the tropics than the subtropics (Xie et al. 2010). Meanwhile, an eastward shift in mean precipitation together with a weakening of the Walker cell was reported over the tropical Pacific for the majority of current climate models (Vecchi et al. 2006; Vecchi and Soden 2007).

Several mechanisms have been proposed to understand the observed and model projected weakening of the Walker cell. One is ascribable to the different increase rate between precipitation and water vapor (Held and Soden 2006). In agreement with the Clausius–Clapeyron relationship, the water vapor increases by roughly 7% per degree of global warming as the relative humidity remains rather constant. However, the precipitation increases at a much lower rate of about 2%–3% per degree of global warming so that the global convective mass fluxes have to be weakened (Held and Soden 2006). The above argument is further applied to the regional tropical Pacific to explain the weakened Walker circulation (Vecchi et al.

2006; Vecchi and Soden 2007) although it is still under debate (Sandeep et al. 2014). The root cause related to this mechanism can be attributed to the fact that the precipitation change is strongly constrained by the radiation change, which evolves much more slowly than the moisture change. A recent study highlighted the role of the mean vertical advection of anomalous vertical potential temperature gradient and further argued that tropical mean SST warming dominates the relative SST pattern in driving the Walker circulation change by analyzing the velocity potential change over the tropics (Ma et al. 2012). We will discuss the linkage of the above two mechanisms in this paper. Meanwhile, the role of weakened zonal SST gradients has been emphasized for the slowdown of the Walker circulation, in particular for twentieth-century observations (Tokinaga et al. 2012a,b; Sandeep et al. 2014).

Disentangling the causality in a strongly coupled climate system is usually difficult. On the one hand, increase of anthropogenic GHG is expected to directly alter radiation, precipitation, and atmospheric circulation. On the other hand, the resultant SST warming can in turn feed back to change the radiation, precipitation, and circulation. The first (second) process is typically very fast (slow) and can be referred to the direct (indirect) effect. The equilibrium climate is a state representing the total climate change, which is the sum of both slow and fast responses (e.g., Bala et al. 2010). The direct effect owing to the increase of GHG (without SST change) has been studied focusing on the precipitation and tropical cyclone changes (e.g., Sugi and Yoshimura 2004; Held and Zhao 2011). However, to the best of our knowledge, how the increased GHG directly impacts the Walker circulation or trade winds remains elusive. One objective of this study is to explore the direct and indirect impacts on the trade wind change owing to an increase in GHG concentration.

Theoretically, the Walker circulation consists of two branches of vertical motion in the Maritime Continent and eastern Pacific and the other two branches of equatorial zonal flows in the lower and upper troposphere, forming a circulation cell system. Usually, the Walker circulation is measured by the sea level pressure (SLP) difference between the western warm pool and eastern cold tongue (e.g., Vecchi et al. 2006; Tokinaga et al. 2012b; DiNezio et al. 2013). One reason is the strong dynamical linkage between zonal SLP gradient and zonal wind/wind stress (Clarke and Lebedev 1996; Vecchi et al. 2006). The other consideration is that the SLP data are relatively reliable while surface winds data could be problematic, in particular for studying the long-term variability (Vecchi et al. 2006). However, use of the zonal SLP gradient for measuring the Walker cell strength has limitations too. First, it

has an implicit assumption that the zonal winds are largely balanced by the zonal SLP gradient, which works only near the equator within the boundary layer. Second, the zonal SLP gradient index cannot describe the detailed spatial structure of trade wind change at specific locations from the western to the eastern Pacific.

Investigation of the change in surface trade winds can be regarded as another measure of the Walker circulation, which has important implications for understanding future climate change on both local and global scales. For example, it has potential impacts on El Niño–Southern Oscillation (ENSO) property changes because both the equatorial mean upwelling and the zonal tilt of thermocline depth are dominantly governed by the amplitude of trade winds; it also plays an essential role in determining the warming rate over the tropical Pacific as well as the globe (e.g., [Kosaka and Xie 2013](#)). In this paper, we aim to examine the GHG-induced change in zonal winds over the equatorial Pacific, and offer an explanation in the trade wind change along with discussion of the uncertainty source.

This paper is organized as follows. [Section 2](#) introduces the models, experiments, and methodology. In [section 3](#), we explore the projected tropical Pacific mean state change due to anthropogenic GHG forcing by focusing on the equatorial Pacific trade winds. The possible physical mechanisms governing the trade wind change associated with GHG forcing are investigated in [section 4](#). [Section 5](#) documents the uncertainty and the source of uncertainty for the equatorial Pacific trade wind change. The last section is the summary and discussion.

2. Model, experiments, and methodology

In this study, we examine 19 climate models that participated in Coupled Model Intercomparison Project phase 5 (CMIP5) ([Taylor et al. 2012](#)); the models and their expansions are listed in [Table 1](#). The projected future change is estimated based on the representative concentration pathway (RCP) 4.5 simulations for the period 2071 to 2099 relative to the corresponding historical simulations for the period 1980 to 2005. The radiative forcing achieved around 2090 in the RCP4.5 scenario is approximately equivalent to that produced by a doubling of CO₂.

We also use a coupled model, POEM [named for its constituent elements, the Parallel Ocean Program (POP), the Ocean Atmosphere Sea Ice Soil (OASIS) coupler, and ECHAM; [Xiang et al. \(2012\)](#)], and its atmospheric-only component ECHAM (v4.6) ([Roeckner et al. 1996](#)). For ECHAM, we use T42 horizontal resolution with 19 sigma levels in the vertical. POEM is a newly developed atmosphere–ocean coupled model that couples

the POP ocean model and ECHAM atmospheric model through the OASIS coupler ([Xiang et al. 2012](#)). We use a relatively coarse resolution of ocean model with 100×116 grid points in the horizontal and 25 levels in the vertical. We apply a SST correction over the equatorial central Pacific and southeast Pacific to artificially eliminate the commonly seen mean SST bias associated with the double intertropical convergence zone (ITCZ) problem ([Xiang and Wang 2013](#); [Xiang et al. 2014](#)). Two coupled model experiments are performed. The first is a 50-yr control run (CTRL). The second is a 50-yr double CO₂ run ($2 \times \text{CO}_2$) and we use the last 20-yr mean as an equilibrium state to study the GHG effect. To show the time evolution of trade winds with GHG forcing, we also perform experiments during the first four years with double CO₂ forcing with each having 30 ensemble members. For example, the first year (year 1) runs are initiated from 30 members of CTRL experiments with each starting from 1 January and then integrated for 1 year. In other words, the first year run and the control run share the same initial conditions but the first year run has double CO₂ effect. The second year (year 2) runs start with the initial conditions generated from the first year runs at the end of their one year integrations. The difference between the first year run and CTRL run represents the first year's response and the difference between the second year run and the first year run shows the second year's response.

To verify the possible mechanisms for trade wind changes, we carry out three atmospheric general circulation model (AGCM) experiments by using ECHAM. The first is a control run forced by climatological SST and sea ice concentration. The second is similar to the control but with double CO₂ forcing. The third is similar to the control except with the SST uniformly warmed by 1.59°C, which is estimated based on the tropical mean SST difference (averaged within 30°S and 30°N) between coupled model experiments $2 \times \text{CO}_2$ and CTRL. The last one is a relative SST forcing experiment with the SST forcing pattern obtaining from the difference between $2 \times \text{CO}_2$ and CTRL but removing the tropical mean SST. The last two experiments adopt the same CO₂ concentration as in the control run. Each AGCM experiment is carried out for 20 years and we analyze the results for the last 18 years.

Following [Ma et al. \(2012\)](#), we use the following thermodynamic equation to understand the physical processes for the circulation change:

$$\frac{\partial T'}{\partial t} + B\omega' \frac{\partial \bar{\theta}}{\partial p} = \frac{Q'}{C_p} - B\bar{\omega} \frac{\partial \theta'}{\partial p}, \quad (1)$$

TABLE 1. Brief description of 19 CMIP5 models used in this study.

Coupled model acronym	Model; institution	AGCM resolution
ACCESS1.0	Australian Community Climate and Earth-System Simulator, version 1.0; Commonwealth Scientific and Industrial Research Organization (CSIRO) and Bureau of Meteorology, Australia (BOM)	$1.875^\circ \times 1.25^\circ$
BCC_CSM1.1	Beijing Climate Center (BCC), Climate System Model, version 1.1; BCC, China Meteorological Administration	$2.8125^\circ \times 2.8125^\circ$
CanESM2	Second Generation Canadian Earth System Model; Canadian Centre for Climate Modeling and Analysis (CCCma)	$2.8125^\circ \times 2.8125^\circ$
CCSM4	Community Climate System Model, version 4; National Center for Atmospheric Research (NCAR)	$1.25^\circ \times 0.9375^\circ$
CNRM-CM5	Centre National de Recherches Météorologiques (CNRM) Coupled Global Climate Model, version 5; CNRM and Centre Européen de Recherche et Formation Avancées en Calcul Scientifique (CERFACS)	$1.40625^\circ \times 1.40625^\circ$
CSIRO-Mk3.6.0	CSIRO Mark, version 3.6.0; CSIRO and the Queensland Climate Change Centre of Excellence (QCCCE)	$1.875^\circ \times 1.875^\circ$
GFDL-CM3	Geophysical Fluid Dynamics Laboratory (GFDL) Climate Model, version 3, and GFDL Earth System Model with Modular	$2.5^\circ \times 2^\circ$
GFDL-ESM2M	Ocean Model 4 (MOM4) component; NOAA GFDL	$2.5^\circ \times 2^\circ$
GISS-E2-R	Goddard Institute for Space Studies (GISS) Model E, coupled with the Russell ocean model; NASA GISS	$2.5^\circ \times 2^\circ$
HadGEM2-CC	Hadley Centre Global Environment Model, version 2–Carbon	$1.875^\circ \times 1.24^\circ$
HadGEM2-ES	Cycle and –Earth System; Met Office Hadley Centre (MOHC)	$1.875^\circ \times 1.24^\circ$
INM-CM4	Institute of Numerical Mathematics (INM) Coupled Model, version 4.0; INM	$2^\circ \times 1.5^\circ$
IPSL-CM5A-LR	L’Institut Pierre-Simon Laplace (IPSL) Coupled Model, version 5, coupled with NEMO, low resolution, and mid	$3.75^\circ \times 1.875^\circ$
IPSL-CM5A-MR	resolution; IPSL	$2.5^\circ \times 1.258^\circ$
MIROC5	Model for Interdisciplinary Research on Climate (MIROC), version 5,	$1.40625^\circ \times 1.40625^\circ$
MIROC-ESM	and MIROC, Earth System Model; Atmosphere and Ocean Research Institute (University of Tokyo), National Institute for Environmental Studies, and Japan Agency for Marine–Earth Science and Technology	$2.8125^\circ \times 2.8125^\circ$
MPI-ESM-LR	Max Planck Institute Earth System Model, low resolution; Max Planck Institute for Meteorology	$1.875^\circ \times 1.875^\circ$
MRI-CGCM3	Meteorological Research Institute (MRI) Coupled Atmosphere–Ocean General Circulation Model, version 3; MRI	$1.125^\circ \times 2.25^\circ$
NorESM1-M	Norwegian Earth System Model, version 1 (intermediate resolution); Norwegian Climate Centre	$2.5^\circ \times 1.875^\circ$

where T' is tropospheric air temperature change, $\bar{\theta}$ and θ' are mean potential temperature and potential temperature change, p is pressure, and $B = (P/P_s)^{R/C_p}$, where P_s is surface pressure, R is the gas constant for air, and C_p is the specific heat at constant pressure. Also, Q is a heating term including longwave and shortwave radiation, surface sensible heat flux, and the latent heat released due to precipitation. Here we omit the horizontal advection term because of the small temperature gradients in the tropics, but keep another small term, the temperature change tendency term, because weak temperature change may induce significant geopotential height and circulation change. The role of the vertical advection term associated with dry static stability change has been noticed for a long time in understanding the tropical climate change (Knutson

and Manabe 1995). Here this term is further separated into two terms, $B\omega'\partial\bar{\theta}/\partial p$ and $B\bar{\omega}\partial\theta'/\partial p$, and the mean advection of anomalous potential temperature change ($B\bar{\omega}\partial\theta'/\partial p$) is moved to the rhs of the equation since it can be regarded as a forcing term from the atmospheric perspective given its tight relationship with SST change (Ma et al. 2012; Muller and O’Gorman 2011).

3. Mean state change over the tropical Pacific

In this section we analyze the projected changes of the mean state in 19 CMIP5 models and POEM by focusing on the equatorial Pacific trade winds. Figure 1 presents changes in mean SST, precipitation, and 850-hPa winds. Consistent with the previous studies (Liu et al. 2005; Lu and Zhao 2012; Xie et al. 2010; Ma and Xie 2013; Lee

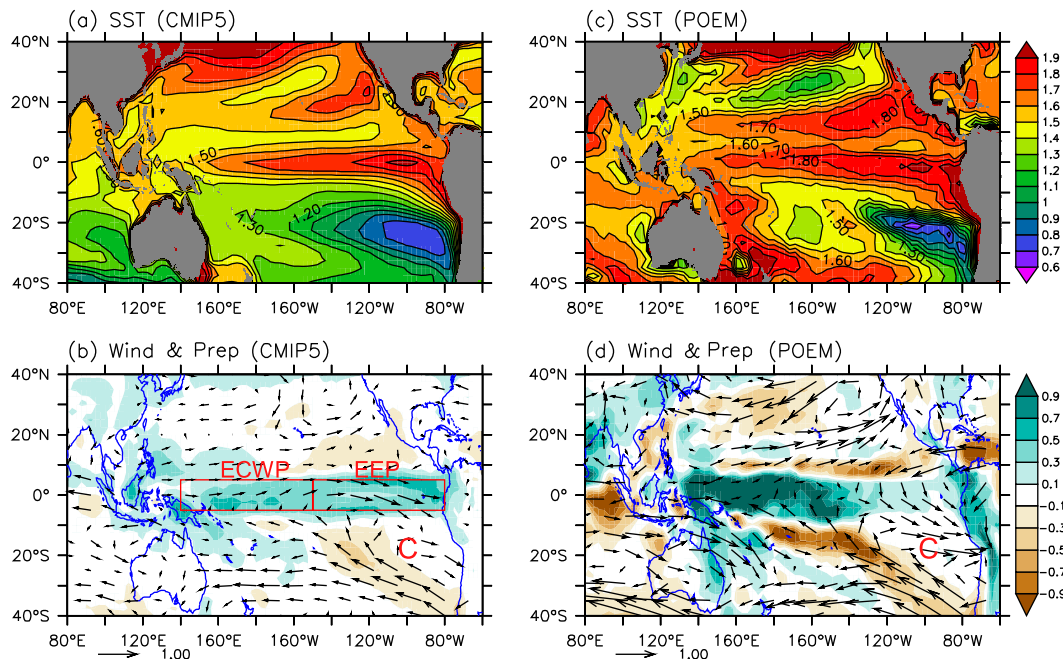


FIG. 1. The multimodel ensemble (MME) mean of (a) SST ($^{\circ}\text{C}$) and (b) precipitation (shading, mm day^{-1}), 850-hPa wind (vectors, m s^{-1}) changes between the RCP4.5 simulations (2071–99) and the historical simulations (1980–2005) from 19 CMIP5 models. (c),(d) As in (a),(b), but for the double CO_2 experiments results comparing with the control run using POEM. The last 20 yr are used with a 50-yr integration for the double CO_2 experiment. The domains for ECWP and EEP are also shown in (b). The red letter C in (b) and (d) represents cyclonic circulation change.

and Wang 2014; Lee et al. 2014), conspicuous warming is found over the equatorial Pacific, extending from the far equatorial eastern Pacific (EEP) to the equatorial western Pacific. Over the subtropical Southern Hemisphere, two minimum warming centers are evident over the southeast Pacific and Indian Ocean (Fig. 1a). Several narrow bands of SST structures appear in the North Pacific. Precipitation increases over the equatorial Pacific and the northwestern Pacific (Fig. 1b). Change in 850-hPa winds is characterized by a conspicuous westerly over the equatorial Pacific, inferring a weakening of the Walker circulation. Of particular note is that a cyclonic anomaly occurs over the southeast tropical Pacific (SETP) concurrent with considerable westerly winds over the EEP (Fig. 1b). The broad features of the change in SST, precipitation, and 850-hPa winds from POEM bear similar resemblance to the CMIP5 models (Figs. 1c, d), justifying an investigation of the mechanisms of weakening trades using this model.

The 19-model MME projects a decrease of mean trade winds by 0.30 m s^{-1} over the equatorial Pacific (5°S – 5°N , 140°E – 80°W) during 2071–99, which corresponds to about 3.2% reduction per degree of global warming.

The wind change can be decomposed into rotational and divergent wind components based on the streamfunction

and velocity potential. As depicted in Fig. 2a, a positive streamfunction center is located over the SETP, and the associated salient zonal winds appear over the EEP. The velocity potential change indicates noticeable divergence (convergence) over the Maritime Continent (SETP), collocating a descending (ascending) motion over the Maritime Continent (SETP). The slackened trade winds (averaged over 5°S – 5°N) are dominated by the rotational winds although the divergent winds also have a contribution (Fig. 2c). Averaged over the equatorial Pacific (140°E – 80°W), the rotational winds are about 4 times larger than the divergent component. The divergent wind change shows a zonally uniform westerly, while the rotational wind change exhibits a maximum over the far EEP. Similar results are obtained for zonal wind change averaged over 2°S – 2°N , confirming the robustness of the above results. Examination of change in 850-hPa geopotential height (H_{850}) reveals a conspicuous relative low pressure center residing in the SETP.

The tropical circulation can be both dynamically and thermally driven. On the one hand, both the radiation and dry static stability change result in an ascending motion change in the mean subsidence region (Held and Soden 2006; Huang et al. 2013). The induced vertical motion change (ω') further leads to low-level convergence as well as the cyclonic circulation in the SETP via a dynamic

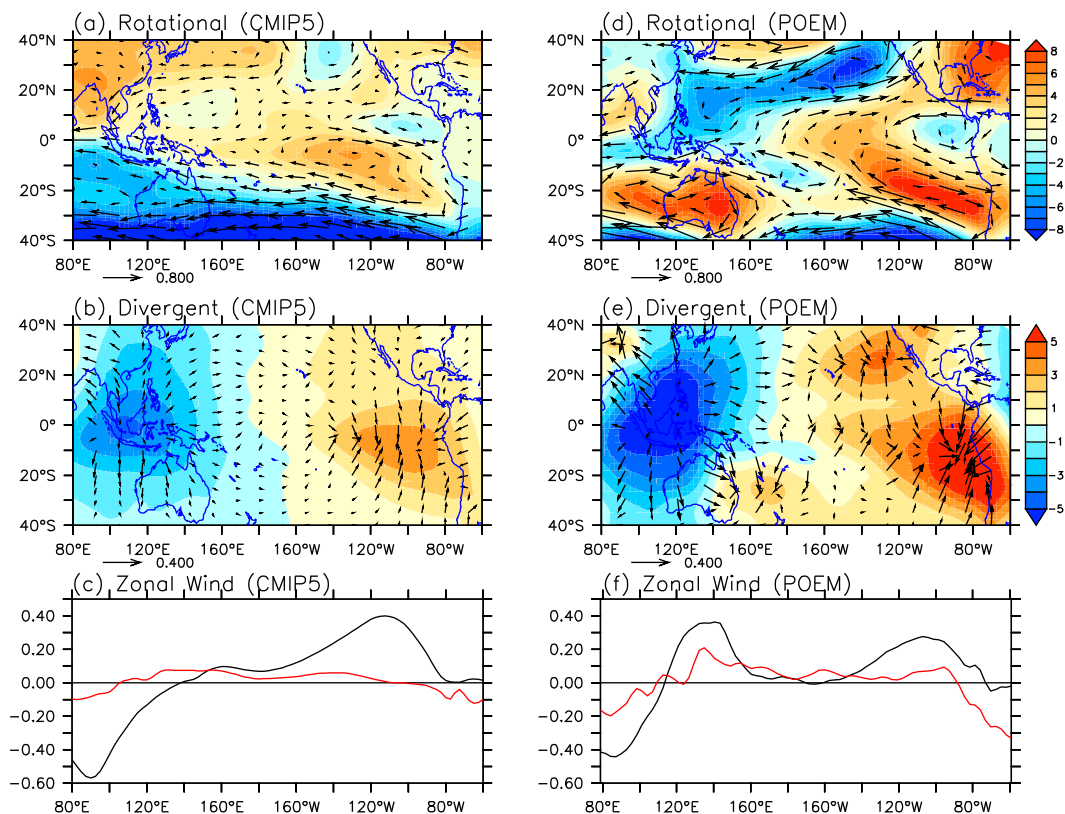


FIG. 2. (left) As in Fig. 1, but for the changes of streamfunction (shading) and (b) velocity potential and the corresponding 850-hPa (a) rotational winds and (b) divergent winds from CMIP5 models; (c) the equatorial (5°S–5°N) zonal rotational (black) and divergent (red) wind change. (right) As at (left), but for POEM results.

effect. On the other hand, the tropospheric temperature change (T') may also partly explain the relative low H_{850} over the SETP via a thermodynamic effect. These two effects are reflected by two terms from the lhs of the thermodynamic equation (1). Figure 3b shows the vertically integrated (from 300 to 850 hPa) temperature pattern (after removing the tropical mean averaged over 30°S–30°N), featuring a robust east–west zonal contrast pattern with relatively more warming over the eastern Pacific than western Pacific. Meanwhile, a maximum warming center is collocated with the relative low H_{850} in the SETP (Fig. 3b). However, the lower-tropospheric (below 850 hPa) temperature change pattern closely follows the SST change pattern. The relative warming of vertically integrated temperature change over the SETP seems to be important for the generation of the local relatively low H_{850} , promoting the weakening of easterlies over the EEP.

4. Understanding what governs the trade wind change

Detection of the root cause of the trade wind change in a fully coupled system is challenging since it involves

direct/fast atmospheric adjustment (without SST change) and indirect/slow atmosphere–ocean coupled (with SST change) effects and also complex feedbacks. In this section, we carried out AGCM experiments using ECHAM (v4.6), the atmospheric component of POEM, to investigate the direct/fast response due to GHG forcing, and also the SST warming-induced indirect/slow response. The atmospheric slow response due to SST-warming forcing can be further decomposed into the tropical mean SST forcing (1.59°C) and the relative SST forcing deviated from the tropical mean SST.

a. Transient response due to double CO_2 forcing

The fast response with CO_2 doubling shows suppressed precipitation over most of the tropical ocean areas in order to balance the reduced radiative cooling effect (Fig. 4). The most pronounced reduction of precipitation is found over the equatorial Pacific near 160°E with a southeastward elongated pattern. It is interesting that the precipitation is suppressed but the trade winds over the ECWP are actually intensified. The suppressed convection over the equatorial Pacific can well explain the intensified trade winds west of the international date

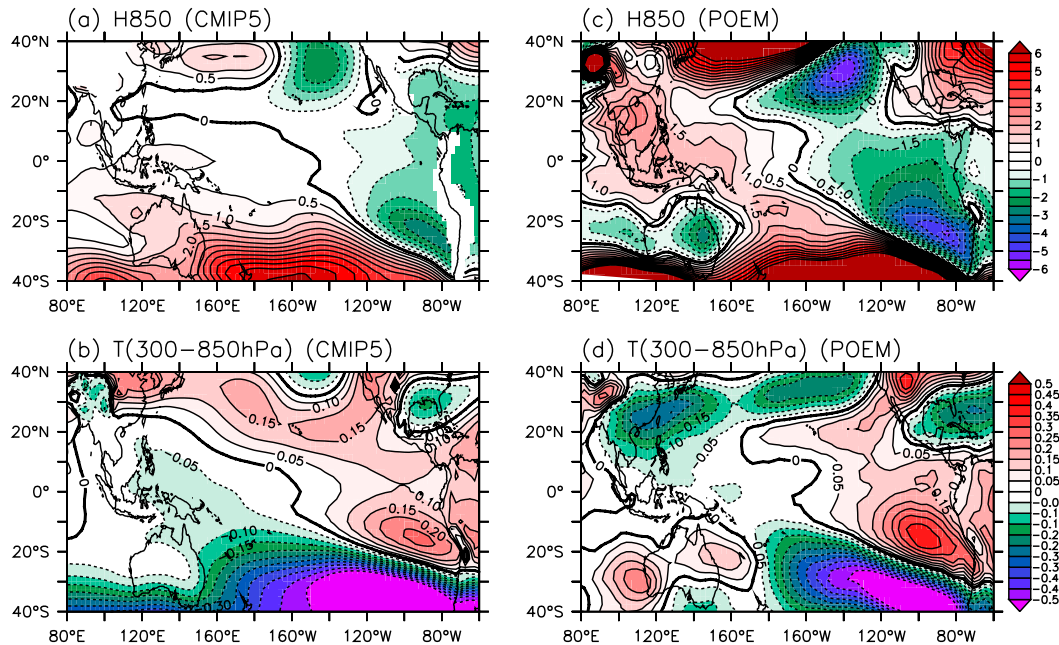


FIG. 3. As in Fig. 1, but for changes of (top) 850-hPa geopotential height and (bottom) temperature averaged from 300 to 850 hPa. Note that the tropical mean (30°S–30°N) has been removed for these two fields.

line. However, the easterly wind change east of date line acts as one component of the intensification of South Pacific subtropical high (Li et al. 2013), which may be also linked to the suppressed convection over South Pacific (Fig. 4a). Although a weak cyclonic circulation and relatively large top of atmosphere (TOA) radiation are seen in the SETP (Fig. 4b), the local maximum of column integrated temperature is absent (Fig. 4c). By contrast, a large area of relative tropospheric cooling is observed in the central tropical Pacific (Fig. 4c), in agreement with the suppressed precipitation and the resultant less latent heat release. In the EEP, there are weak westerly winds and cyclonic circulation change, suggested to be mainly driven by the dynamic effect with local ascending motion change (not shown). The tropospheric temperature change does not show clear local maximum warming (Fig. 4c) because the vertical potential temperature gradient change is very small in the Atmospheric Model Intercomparison Project (AMIP) run with double CO₂ forcing. Thus the dominant terms balanced each other in the thermodynamic equation are radiation and dry adiabatic cooling associated with the ascending motion change.

b. Atmospheric response to the uniform SST warming forcing

Comparing with the control run, the uniform warming experiment generally produces a wet-get-wetter and dry-get-drier precipitation pattern (Fig. 5a). In the western

North Pacific, the intensified precipitation tends to drive westerly winds over the equatorial western Pacific. Meanwhile, a cyclonic circulation is confined over the SETP accompanied by salient westerly winds over the EEP (Fig. 5a). This cyclonic circulation is collocated with a column integrated (300–850 hPa) relative warming center over the SETP (Fig. 5c), consistent with the coupled model results (Figs. 3b,d). As mentioned above, the relative tropospheric (300–850 hPa) warming in the SETP is essential to form the cyclonic circulation as well as the equatorial westerly in the EEP.

The question then arises as to what causes the maximum column integrated temperature warming over the SETP. Here we also assume that the horizontal advection term is small because of the small temperature gradients in the tropics. The TOA radiative forcing effect cannot explain the maximum warming over the SETP (Fig. 5b). The surface sensible heat flux is neglected since it has less contribution to the free-tropospheric temperature change (Ma et al. 2012). Associated with the cyclonic circulation over the SETP, lower-level convergence (Figs. 2b,e) and the ascending motion (not shown) tend to generate adiabatic cooling in the absence of local precipitation heating change (Fig. 1).

Therefore, the largest term contributing to the relative warming in the SETP has to be the mean vertical advection of anomalous warm air from the upper troposphere downward to warm the lower troposphere. Associated with anthropogenic GHG forcing, the most

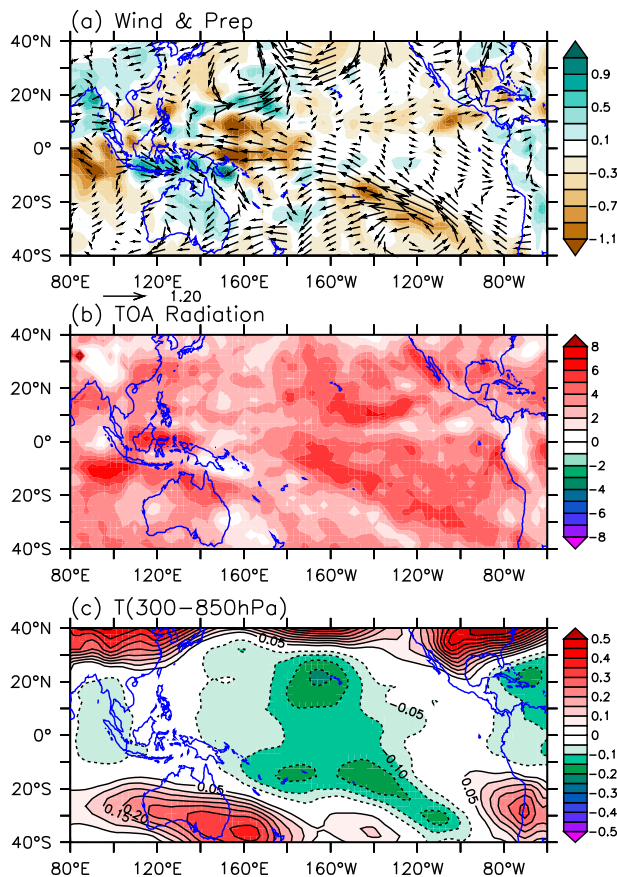


FIG. 4. Atmospheric response to double CO_2 forcing with the prescribed climatological SST and sea ice forcing: (a) precipitation (shading, mm day^{-1}) and 850 hPa wind, (b) top of atmosphere (TOA) radiation change (W m^{-2}) including both outgoing long-wave radiation and net shortwave radiation, and (c) column integrated temperature change averaged from 300 to 850 hPa with the tropical mean (30°S – 30°N) removed. The atmospheric model used here is ECHAM.

pronounced warming is taking place in the tropical upper troposphere, resembling a quite uniform horizontal distribution (Fig. 6a). This is a very robust feature among the current state-of-the-art models due to the moist adiabatic adjustment and wave adjustment (Knutson and Manabe 1995). The upper-tropospheric warming can influence the lower-tropospheric circulation in the presence of mean subsidence, such as the EEP over the subsiding branch of the mean Walker circulation. The key system that bridges the upper-tropospheric warming and the lower-level wind change is the mean subsidence, acting as a draining tube to “suck” the upper-tropospheric warm air downward to warm the mid to lower troposphere. Similar to the double CO_2 effect, an anomalous upward motion is also found near the coast of South America favoring the formation of cyclonic circulation in the SETP (not

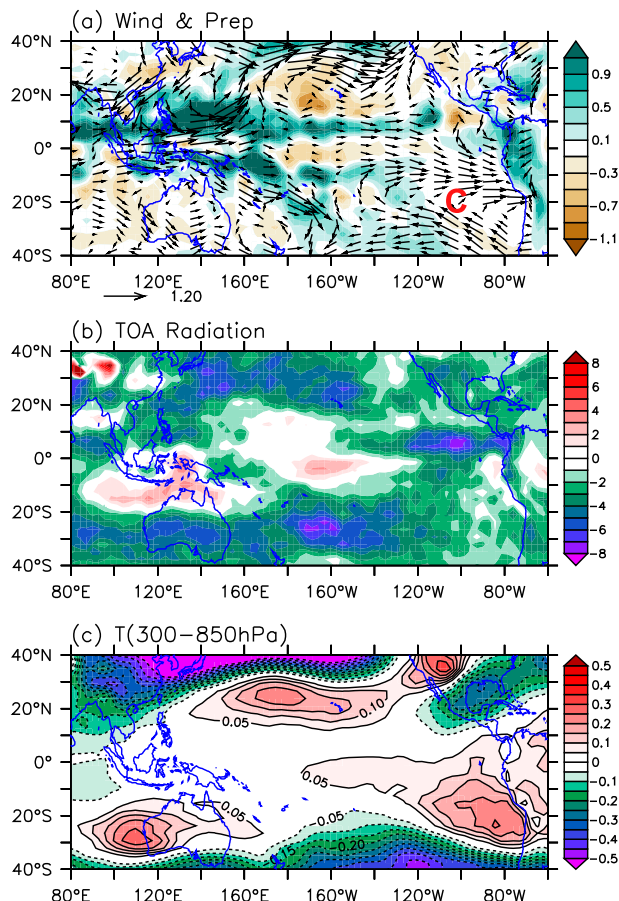


FIG. 5. As in Fig. 4, but for the uniform tropical mean SST warming forcing (1.59°C).

shown). Given the negative TOA radiation effect, the ascending motion is also attributed to the forcing effect from the mean advection of vertical potential temperature gradient change based on Eq. (1). This can be referred to as a “top-down” mechanism, and this effect has been emphasized by Ma et al. (2012) in which they refer to this as the mean advection of stratification change (MASC). This top-down mechanism largely explains the ascending motion change through altering the dry static stability, consistent with previous studies (e.g., Held and Soden 2006; Huang et al. 2013). Meanwhile, it warms the tropospheric temperature and favors a relatively low pressure and cyclonic circulation system at the lower troposphere over the SETP.

c. Atmospheric response to the relative SST forcing

The experiment with the relative SST pattern forcing induces pronounced cross-equatorial flow because of the meridional SST gradient (Fig. 7). Meanwhile, the westerly wind anomaly prevails from the equatorial western Pacific to EEP, together with enhanced precipitation

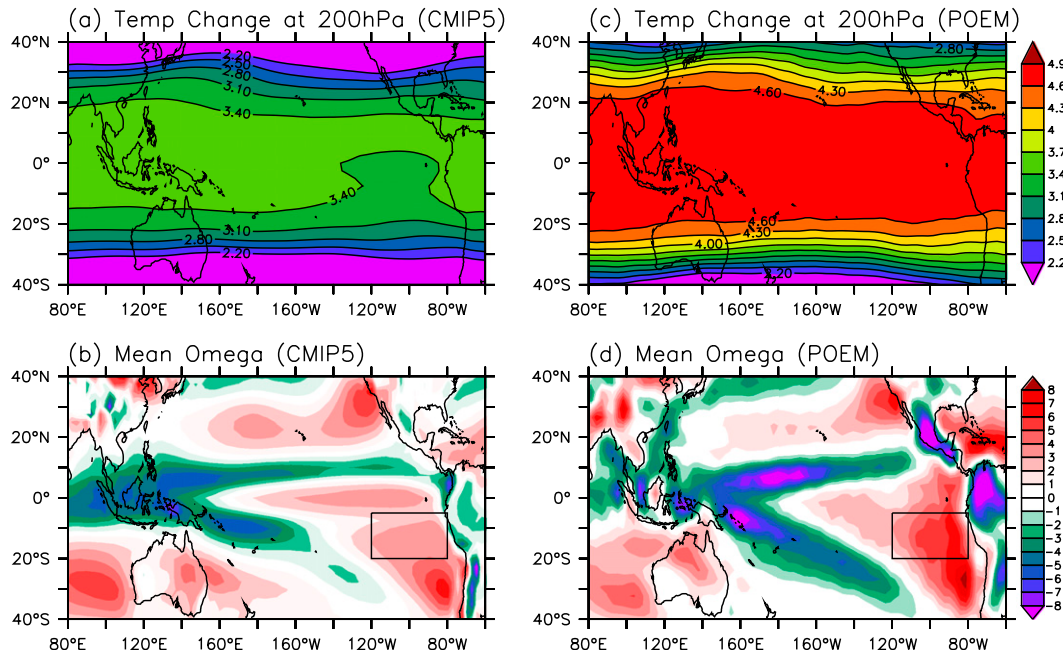


FIG. 6. Changes of upper-tropospheric (200 hPa) temperature ($^{\circ}\text{C}$) from (a) the MME of CMIP5 models and (c) POEM. Also shown are the long-term mean vertical velocity ($10^{-2} \text{ Pa s}^{-1}$) at 500 hPa from (b) MME of CMIP5 models and (d) POEM. The negative denotes ascending motion, and vice versa. Black boxes in (b) and (d) show the key region in driving the cyclonic circulation associated with mean subsidence.

(Fig. 7b). The westerly wind anomaly over the equatorial Pacific can be driven directly by the weakened zonal SST gradient and also the local enhanced precipitation. Different from the uniform SST warming forcing experiment, the relative tropospheric temperature warming (Fig. 7d) and vertical motion change in the SETP are very weak. Meanwhile, the TOA radiation change (Fig. 7c) mainly reflects the deep-convection-related cloud change, having less contribution to the tropospheric temperature and circulation change.

For the convenience of intermodel comparison in the following section, we propose one index as a proxy representing the contribution from the relative SST pattern to the weakening of trade winds: the relative SST warming over the equatorial Pacific (5°S – 5°N , 140°E – 80°W) [i.e., the deviation from the tropical mean (30°S – 30°N) SST] normalized by its tropical mean SST change. The reason is twofold. First, the gross moist instability tightly follows the relative SST pattern as the upper-tropospheric temperature change is rather spatially uniform (Xie et al. 2010). Hence the relative SST warming over the equatorial Pacific tends to cause local enhanced convection as well as westerly winds. Second, the majority of the CMIP5 models produce an El Niño-like warming pattern with more warming in the far EEP than the ECWP. Therefore, a larger relative SST over the equatorial Pacific typically implies more intensified

local convection but reduced zonal mean SST gradient, ending up with more slackened trade winds.

d. Time evolution of trade wind change in response to double CO_2 forcing

The above three subsections showed how the atmosphere responds to the direct/fast CO_2 forcing and indirect/slow SST forcing. In reality, the atmospheric response at the equilibrium state may not be exactly the sum of the above three processes owing to the existence of non-linearity in the system. Here we also examine the time evolution of trade winds in response to double CO_2 forcing using the coupled model POEM.

In the first year (year 1), the atmospheric response is very similar to the AMIP run with fixed SST forcing (cf. Figs. 8d and 4a), characterized by suppressed precipitation but intensified trade winds over the ECWP. The suppressed convection over the off-equatorial region may also contribute to the easterly winds over the ECWP. In the EEP, a westerly wind anomaly is also obvious (Fig. 8d). The SST pattern displays less warming over the ECWP but more warming over the EEP, which is also linked to the fact that the mean winds are smaller there so that the latent heat flux damping is relatively smaller compared with that in the equatorial central Pacific. In the second year (year 2), the ECWP is still dominated by easterly winds but with reduced amplitude, while an

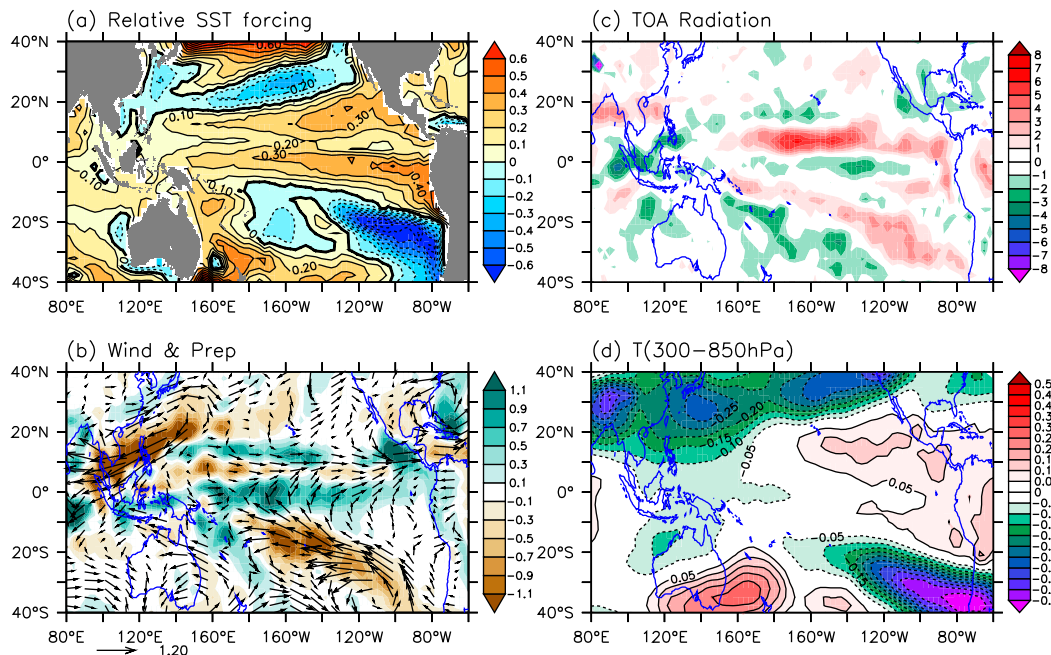


FIG. 7. (b)–(d) Similar to (a)–(c) in Fig. 4 but for (a) the relative SST forcing deviated from the tropical mean (30°S–30°N). The anomalous SST forcing is derived from the SST change between experiments $2 \times \text{CO}_2$ and CNTL using POEM (Fig. 1c).

anomalous cyclonic circulation becomes conspicuous in the SETP (Fig. 8e). The maximum of suppressed precipitation retreats southeastward compared with the first year, while intensified precipitation become more pronounced west of 160°E. We argue that the wind change is both associated with the tropical mean SST change (from 0.24° to 0.59°C) and relative SST change over the equatorial Pacific (from -0.05° to 0.03°C). For year 4, the SST warming pattern has been well established compared to the equilibrium state. The meridional SST pattern also shows more warming in the northeastern Pacific but less warming over the southeast Pacific (Fig. 8c). The region with enhanced precipitation and westerly wind change are expanding farther eastward accompanied by the westerly wind change (Fig. 8f).

Figure 9 illustrates the time evolution of equatorial zonal winds and vertical motion. For year 1, the intensified trade winds and suppressed vertical motion are similar to that in the AMIP run (Fig. 9a), indicative of the dominant role of atmospheric fast/direct response. The westerly winds over the western Pacific first occur in the second year and migrate eastward together with the enhanced convection. This result suggests that the weakened trade winds first take place in the EEP, then occur over the western Pacific, and finally over the equatorial central Pacific with the involvement of strong atmosphere–ocean interaction. Although both fast and slow processes contribute to the westerly winds in the

EEP (Figs. 4a, 5a, 7b), it is not very clear why the zonal winds over the EEP have less change with time evolution (Fig. 9a).

The above experiments show how the SST and surface wind evolve over time with transient double CO_2 forcing. They highlight the importance of direct/fast response to GHG forcing in the coupled model equilibrium state, which has drawn less attention previously. Meanwhile, they also suggest that the atmosphere–ocean coupling and the resultant SST pattern play an important role in regulating the wind change.

5. The uncertainty in trade wind change

The above session suggests three possible processes that are responsible for the equatorial Pacific trade wind change: atmospheric fast adjustment due to CO_2 change, uniform SST forcing, and relative SST pattern forcing. In this section we further investigate the zonal structure of the trade wind change, and then elaborate on the uncertainty of trade wind change and its origins.

a. Discrepancy among model projections of trade winds

We present, in Fig. 10, the equatorial (5°S – 5°N) zonal wind change for 19 individual CMIP5 models and POEM. Although the 19-model ensemble mean experiences a westerly wind change across the entire equatorial Pacific

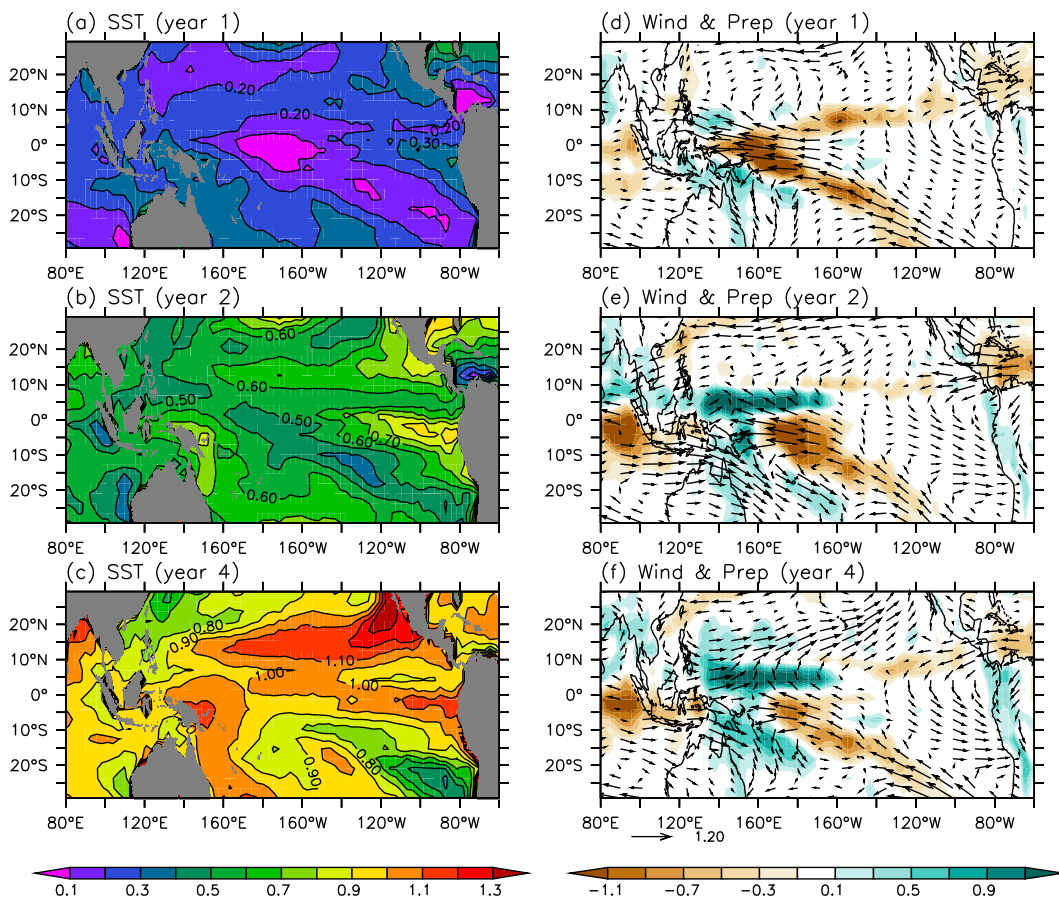


FIG. 8. Time evolution of (left) SST and (right) precipitation (shading) and 850-hPa winds (vectors) with double CO_2 forcing in POEM model during the first four years; 30 ensemble members are used for each experiment.

(red line in Fig. 10), 5 out of 19 models produce zonal mean averaged easterly winds over 5°S – 5°N , 140°E – 80°W . The multimodel-ensemble mean value of the zonal wind change is 0.28 m s^{-1} while the standard deviation of the intermodel spread is 0.56 m s^{-1} , indicating that the zonal wind change is not significant in terms of the signal-to-noise ratio.

We further separate the zonal mean trade winds into two regions, the ECWP (5°S – 5°N , 140°E – 150°W) and EEP (5°S – 5°N , 150° – 80°W). For the zonal mean winds in the EEP, 18 out of 19 models produce anomalous westerly winds, while in the ECWP 10 out of 19 models produce westerly anomalous winds, indicating that conspicuous uncertainty exists in the ECWP. Note that one model produces extremely strong westerly change in the equatorial Pacific (Fig. 10), but the aforementioned conclusion still remains valid if this “outlier” is removed. These results are also robust for the trade wind change at the boundary layer of 1000 hPa (not shown).

In the previous section, we have proposed three different processes contributing to the trade wind change. In the EEP, all these three processes seem to contribute

to the weakened trade wind, which is consistent with the robust change over the EEP for CMIP5 models. In the ECWP, however, the effect from direct/fast response is opposite to that due to indirect/slow response with SST forcing. This to a certain degree accounts for the large uncertainty over the ECWP for CMIP5 models.

Considering the model output availability, we cannot distinguish the intermodel diversity for the direct/fast response due to GHG forcing for the CMIP5 models, but it is definitely one source explaining the uncertainty of relative SST warming pattern as well as the trade wind change over the ECWP. The other two processes associated with SST change are then emphasized here. We plot the scatter diagram of the mean advection of the vertical potential temperature gradient ($-\overline{\partial\theta'}/\partial p$) over the SETP (20° – 5°S , 120° – 80°W) (black boxes in Figs. 6b,d) and the equatorial zonal wind change (Figs. 11a,c). Note that the vertical advection term has large intermodel spread, and their tight relationship is significant (at 99% confidence level) only over the EEP ($r = 0.69$; Fig. 11c) but not over the ECWP ($r = 0.33$; Fig. 11a). Both the mean vertical velocity and vertical

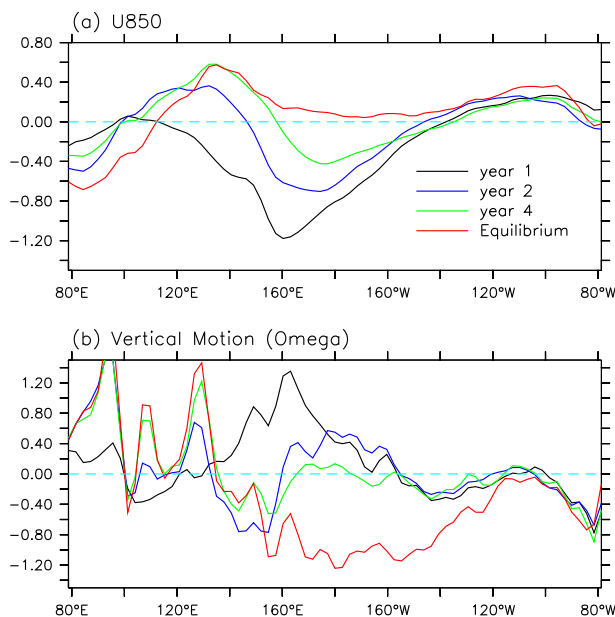


FIG. 9. (a) Equatorial (5°S – 5°N) zonal wind change in the coupled model experiments with double CO_2 forcing during the first four years. (b) As in (a), but for vertical motion change ($10^{-2} \text{ Pa s}^{-1}$).

potential temperature gradient change are significantly correlated with the EEP zonal wind change: $r = 0.62$ and $r = 0.53$, respectively. This result partly reflects the contribution from the tropical mean SST temperature change that shows a tight relationship with the vertical potential temperature gradient with the intermodel correlation ($r = 0.87$). By contrast, the ECWP trade wind change is well correlated with the tropical Pacific relative SST change ($r = 0.80$, Fig. 11b), opposite to that in the EEP ($r = 0.24$, Fig. 11d).

The above results confirm that both uniform warming and relative warming SST patterns can contribute to the weakened trade winds, while the large uncertainty over

the ECWP likely originates from the disparity of the relative SST pattern among different models.

b. Possible root causes of the uncertainty

It is demonstrated that the trade wind change remains of great uncertainty over the ECWP and this uncertainty is tightly linked to model equatorial Pacific SST deviation from the tropical mean. We have made composite analyses by separating the 19 models into two groups: one with weakened (10 models) and the other with intensified trades (9 models) over the ECWP (Fig. 12). In the EEP, both groups show weakening of trades together with a cyclonic circulation over the SETP. As expected, the more weakened trade winds correspond to stronger equatorial Pacific SST warming (Fig. 12).

However, the SST change should not be solely treated as a forcing in a coupled system. From the oceanic point of view, weakened trade winds are also able to induce SST warming over the equatorial Pacific through both thermodynamic and dynamic effects. On the one hand, weakened trade winds tend to lead less evaporation so as to warm the sea surface. On the other hand, weakened trade winds can cause eastward warm advection as well as suppressed cold vertical advection, facilitating the SST warming. Then the key concern is to identify the root cause of the SST pattern so as to understand the uncertainty source of the trade wind change. This is critical to estimate the most likely future change of trade winds and also provides guidance for the improvement of current climate models. But, it is also a very challenging issue since many factors can influence the equatorial Pacific SST warming such as convection, atmosphere–ocean coupling, and feedbacks, as well as the ocean and atmospheric mean states.

A realistic simulation of the current mean climate may provide a necessary (but not sufficient) condition for a reliable future projection. Inspection of mean winds

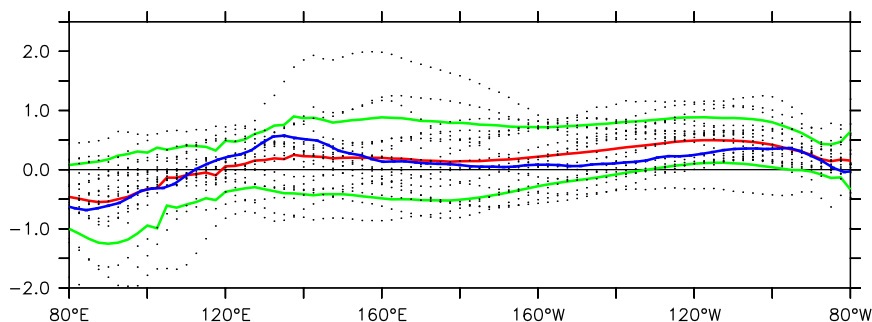


FIG. 10. Equatorial (5°S – 5°N) zonal wind changes from 19 individual CMIP5 models (dotted lines) and the corresponding MME (red). Two green lines show the MME plus/minus one standard deviation of the zonal wind changes for 19 CMIP5 models. The blue line is the equatorial (5°S – 5°N) zonal wind changes from POEM.

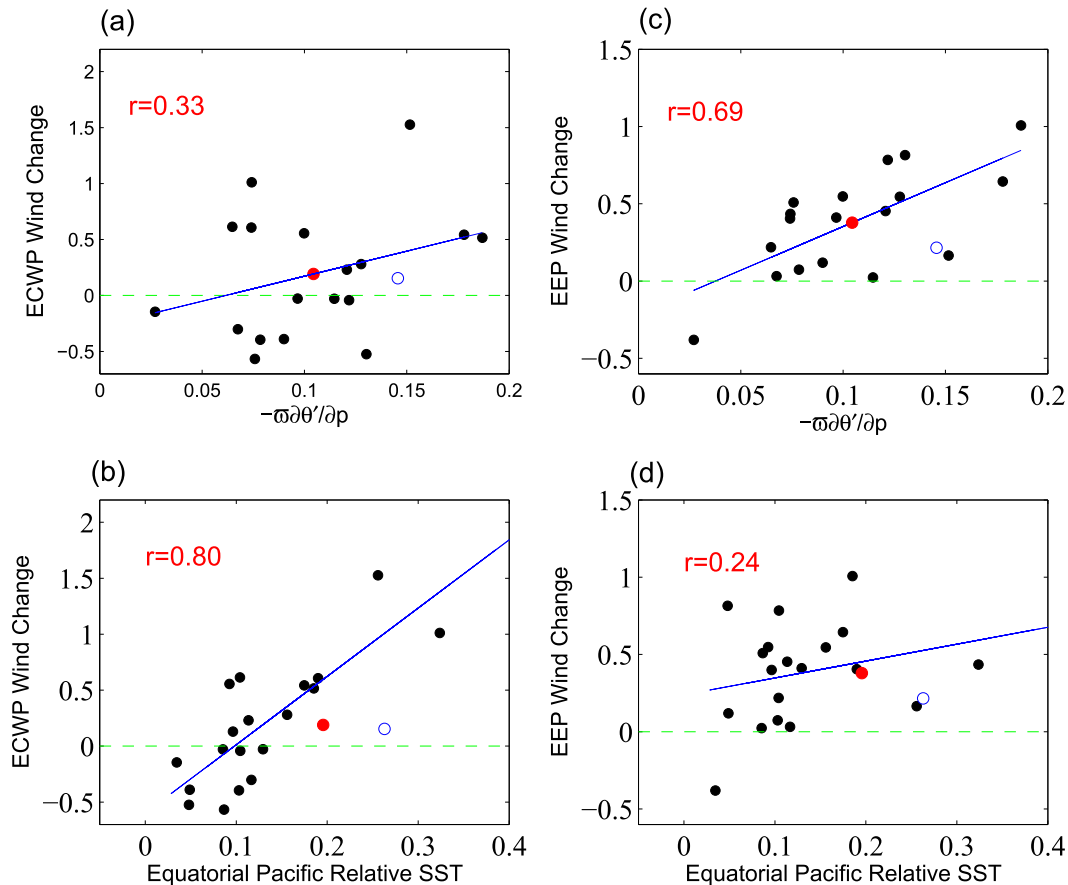


FIG. 11. Scatter diagram between the mean vertical advection of anomalous potential temperature gradient ($-\overline{\omega\partial\theta'}/\partial p$, K day^{-1}) over the southeast tropical Pacific ($20^{\circ}\text{--}5^{\circ}\text{S}$, $120^{\circ}\text{--}80^{\circ}\text{W}$) and the changes of zonal winds over (a) ECWP and (c) EEP. The anomalous vertical potential temperature gradient is roughly estimated from the temperature change between 300 and 850 hPa. (b),(d) As in (a),(c), but for the changes between the equatorial Pacific relative SST ($5^{\circ}\text{S}\text{--}5^{\circ}\text{N}$, $140^{\circ}\text{E}\text{--}80^{\circ}\text{W}$) (deviated from the tropical mean and then normalized by the tropical mean) and the equatorial zonal winds. The red dots denote the MME from MME of 19 CMIP5 models and the blue open circles represent POEM. Owing to data availability, 18 models are used in (a) and (c). The blue lines represent the corresponding linear regression based on CMIP5 models, and the red numbers in the upper left of each panel are the corresponding correlations.

under the current climate is instrumental in understanding the intermodel spread of SST and trade wind changes. Figure 13a shows the composite difference of the long-term mean 850-hPa winds for the historical run between the two groups. The intensified ECWP trade winds group has stronger mean winds than the weakened ECWP trade winds group. The scatter diagram between the mean winds over $5^{\circ}\text{S}\text{--}5^{\circ}\text{N}$, $180^{\circ}\text{--}80^{\circ}\text{W}$ and the zonal wind change in the ECWP corroborates the significant relationship ($r = 0.54$) between the mean winds and projected wind change (Fig. 13b). How do the mean trade winds under current climate determine the future projections of trade wind change? For a model with stronger mean trade winds, it tends to have a larger damping effect on the SST warming over the equatorial Pacific. Along with SST rise, larger mean winds not only give rise to stronger upward

latent heat flux, but also produce stronger mean upwelling and more tilted zonal thermocline, both contributing to a relatively cooler equatorial Pacific through the so-called thermostat cooling effect for future projections (Clement et al. 1996; Cane et al. 1997). Therefore, for the model with stronger mean trades, both the thermodynamic and dynamic effect can result in weaker equatorial Pacific SST warming but more intensified trade winds.

The mean zonal winds over the equatorial central to eastern Pacific ($5^{\circ}\text{S}\text{--}5^{\circ}\text{N}$, $180^{\circ}\text{--}80^{\circ}\text{W}$) vary greatly from one model to the other, ranging from -5 to -10.5 m s^{-1} with their MME of -7.5 m s^{-1} (Fig. 10b). The mean 850-hPa zonal winds ($5^{\circ}\text{S}\text{--}5^{\circ}\text{N}$, $180^{\circ}\text{--}80^{\circ}\text{W}$) from the National Centers for Environmental prediction (NCEP)–Department of Energy (DOE) AMIP-II reanalysis products (1979–2011; Kanamitsu et al. 2002) and the

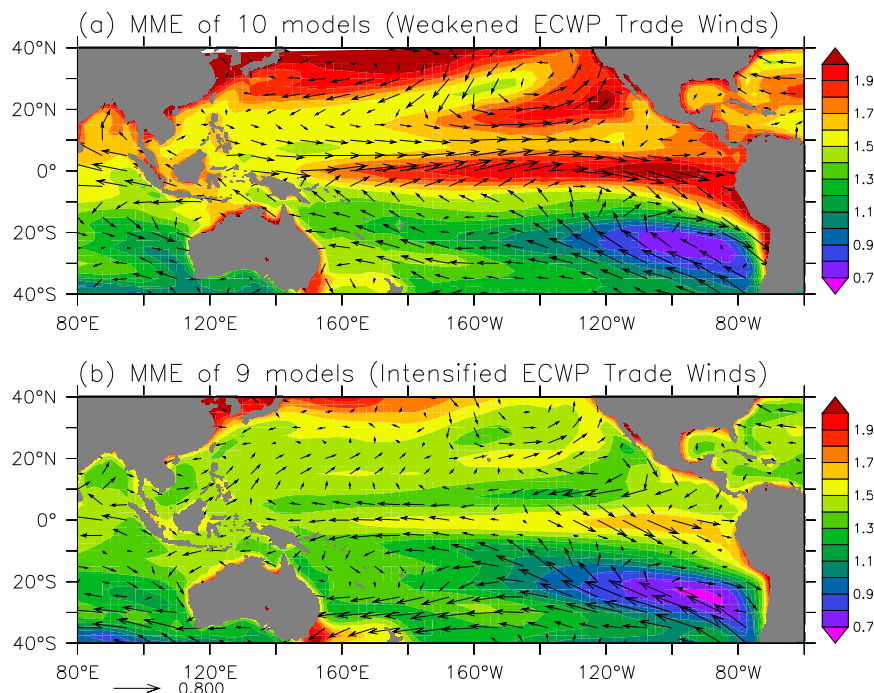


FIG. 12. The MME of SST (shading) and 850-hPa mean wind (vectors) changes for (a) 10 models with weakened ECWP zonal winds and (b) 9 models with intensified ECWP zonal winds.

Interim European Centre for Medium-Range Weather Forecasts Re-Analysis (ERA-Interim) data (1979–2011; [Dee et al. 2011](#)) are about -7.0 and -5.8 m s^{-1} , respectively. These results indicate that mean trade winds are overestimated in the MME of 19 CMIP5 models than observations, which is cohesive with the equatorial Pacific cold SST bias common to current climate models (e.g., [Lin 2007](#)). Note that the MME of 10 models (weakened ECWP trade winds) and 9 models (intensified ECWP trade winds) are -6.5 and -8.5 m s^{-1} , respectively. Comparing the mean winds between CMIP5 models and observations, we suggest that the MME of 10 CMIP5 models with weakened ECWP winds may provide a most likely projection with about 0.63 m s^{-1} reduction of trades over the ECWP at the end of the twenty-first century, while the 19 CMIP5 model MME may underestimate the amplitude of trade wind change. The broad discrepancy of mean trade wind simulation spotlights the importance and necessity to improve coupled model performance for the current climate so as to obtain more reliable future projections.

6. Summary and discussion

The weakened Walker circulation associated with GHG forcing has been extensively studied previously by

focusing on the zonal SLP gradient change or the vertical motion between the Maritime Continent and the far EEP as it is closely linked to the change of precipitation and the hydrological cycle. As one branch of Walker circulation, understanding the change of equatorial Pacific trade winds is also pivotal because it can to a great degree determine the global mean temperature change (e.g., [Kosaka and Xie 2013](#)) and also has potential impacts on ENSO property changes.

Sensitivity experiments demonstrate that the trade wind response involves both direct/fast atmospheric adjustment and indirect/slow atmosphere–ocean coupled adjustment. The direct/fast response tends to enhance the trade winds, especially over the ECWP. By contrast, the SST warming-related indirect/slow process weakens the trade winds, and the uniform (relative) tropical warming facilitates the slackening of trades over the EEP (ECWP). The atmospheric direct/fast response to GHG forcing with enhanced trades is supported by the Geophysical Fluid Dynamics Laboratory global High Resolution Atmospheric Model (HiRAM) ([Zhao et al. 2009](#)) results (not shown). But, the establishment of robustness requires investigation of more climate models in the future.

The MME of 19 CMIP5 models shows weakened trade winds at 850 hPa, that is, a westerly wind anomaly, prevailing from the equatorial western Pacific to the EEP with the maximum over the EEP. The weakened

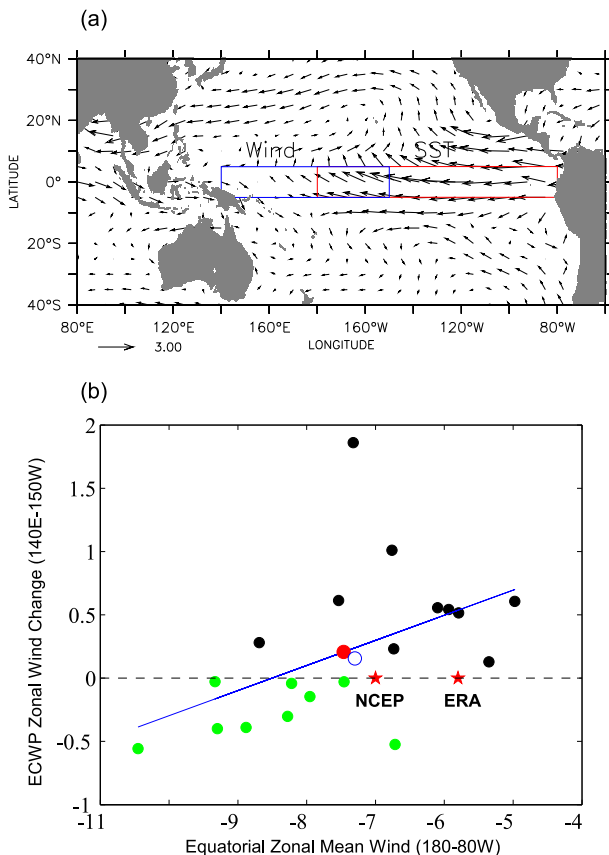


FIG. 13. (a) The 850-hPa mean wind difference (historical runs) between the two groups with weakened (10 models) and intensified (9 models) trade winds. (b) Scatter diagram between the equatorial zonal mean wind (180°–80°W) [red box in (a)] and the projected changes of ECWP (140°E–150°W) zonal winds [blue box in (a)]. The black (green) dots show the weakened (intensified) trade winds over the ECWP. The red dot denotes the MME results and the blue open circle represents the POEM result. The red stars show the observational mean trade winds from NCEP and ERA-Interim. The MME of mean zonal winds over (180°–80°W) for 10 models (weakened ECWP trade winds) and 9 models (intensified ECWP trade winds) are -6.5 and -8.5 m s^{-1} , respectively.

trade winds are only robust over the EEP (5°S–5°N, 150°–80°W) with weak intermodel spread. The robust change of trades over the EEP is driven by both a dynamic effect (vertical motion change) and thermodynamic effect (temperature change). These two effects are both related to the downward advection of upper-tropospheric warming by mean subsidence to form an anomalous low-level cyclonic circulation over the SETP. This top-down mechanism is tightly linked to the tropical mean SST change. This point is also confirmed by a coupled model experiment with a relatively uniform upper-tropospheric heating experiment, which produces strikingly similar surface winds and SST change pattern with the double CO_2 experiment (Xiang et al. 2014;

Xie et al. 2013). Over the ECWP, considerable uncertainty is seen among individual models, with 9 out of 19 models producing intensified trade winds. It is demonstrated that the uncertainty likely originates from the uncertainty of the relative SST over the equatorial Pacific with respect to the tropical mean. Meanwhile, the large intermodel diversity in simulating the mean trade winds under current climate provides one possibility for explaining the intermodel spread of future trade wind change.

This study may give some clues to understand the trade wind change in the twentieth century. Distinguished from modeling future projections (Fig. 1b), the observed weakened trade winds are apparent only over the ECWP but not in the EEP (Fig. 2a in Tokinaga et al. 2012b). There are two possible interpolations based on analysis of model results presented in this study. First, the upward amplification of temperature warming in the troposphere is not confirmed from observations (e.g., Fu et al. 2011) so the top-down mechanism may not be very effective during the studied period in driving the surface wind change especially over the ECWP. Second, the anthropogenic forcing effect may not be as strong as internal variability. For example, the interdecadal Pacific oscillation has been suggested to play an important role in intensifying the Walker circulation during the previous three decades (Dong and Lu 2013).

Acknowledgments. The authors benefitted from discussions with Isaac Held and Shang-Ping Xie. We acknowledge support of this work from Korean Ministry of Education, Science and Technology Grant (MEST 2011-0021927) through the Global Research Laboratory Program and Asia-Pacific Economic Cooperation (APEC) Climate Center (APCC) international project. B. X. was also partly supported by the NOAA MAPP Program under Awards NA12OAR4310075. The authors also acknowledge partial support from International Pacific Research Center, which is sponsored by JAMSTEC.

REFERENCES

- Bala, G., K. Caldeira, and R. Nemani, 2010: Fast versus slow response in climate change: Implications for the global hydrological cycle. *Climate Dyn.*, **35**, 423–434, doi:10.1007/s00382-009-0583-y.
- Cane, M. A., A. C. Clement, A. Kaplan, Y. Kushnir, D. Pozdnyakov, R. Seager, S. E. Zebiak, and R. Murtugudde, 1997: Twentieth century sea surface temperature trends. *Science*, **275**, 957–960, doi:10.1126/science.275.5302.957.
- Christensen, J. H., and Coauthors, 2014: Climate phenomena and their relevance for future regional climate change. *Climate Change 2013: The Physical Science Basis*, T. F. Stocker et al., Eds., Cambridge University Press, 1217–1308.

- Clarke, A. J., and A. Lebedev, 1996: Long-term change in the equatorial Pacific trade winds. *J. Climate*, **9**, 1020–1029, doi:[10.1175/1520-0442\(1996\)009<1020:LTCITE>2.0.CO;2](https://doi.org/10.1175/1520-0442(1996)009<1020:LTCITE>2.0.CO;2).
- Clement, A. C., R. Seager, M. A. Cane, and S. E. Zebiak, 1996: An ocean dynamical thermostat. *J. Climate*, **9**, 2190–2196, doi:[10.1175/1520-0442\(1996\)009<2190:AODT>2.0.CO;2](https://doi.org/10.1175/1520-0442(1996)009<2190:AODT>2.0.CO;2).
- Dee, D. P., and Coauthors, 2011: The ERA-Interim reanalysis: Configuration and performance of the data assimilation system. *Quart. J. Roy. Meteor. Soc.*, **137**, 553–597, doi:[10.1002/qj.828](https://doi.org/10.1002/qj.828).
- Deser, C., A. S. Phillips, and M. A. Alexander, 2010: Twentieth century tropical sea surface temperature trends revisited. *Geophys. Res. Lett.*, **37**, L10701, doi:[10.1029/2010GL043321](https://doi.org/10.1029/2010GL043321).
- DiNezio, P. N., G. A. Vecchi, and A. C. Clement, 2013: Detectability of change in the Walker circulation in response to global warming. *J. Climate*, **26**, 4038–4048, doi:[10.1175/JCLI-D-12-00531.1](https://doi.org/10.1175/JCLI-D-12-00531.1).
- Dong, B., and R. Lu, 2013: Interdecadal enhancement of the Walker circulation over the tropical Pacific in the late 1990s. *Adv. Atmos. Sci.*, **30**, 247–262, doi:[10.1007/s00376-012-2069-9](https://doi.org/10.1007/s00376-012-2069-9).
- Fu, Q., S. Manabe, and C. M. Johanson, 2011: On the warming in the tropical upper troposphere: Models versus observations. *Geophys. Res. Lett.*, **38**, L15704, doi:[10.1029/2011GL048101](https://doi.org/10.1029/2011GL048101).
- Held, I. M., and B. J. Soden, 2006: Robust responses of the hydrological cycle to global warming. *J. Climate*, **19**, 5686–5699, doi:[10.1175/JCLI3990.1](https://doi.org/10.1175/JCLI3990.1).
- , and M. Zhao, 2011: The response of tropical cyclone statistics to an increase in CO₂ with fixed sea surface temperature. *J. Climate*, **24**, 5353–5364, doi:[10.1175/JCLI-D-11-00050.1](https://doi.org/10.1175/JCLI-D-11-00050.1).
- Huang, X., and Coauthors, 2013: A radiative–convective equilibrium perspective of weakening of the tropical Walker circulation in response to global warming. *J. Climate*, **26**, 1643–1653, doi:[10.1175/JCLI-D-12-00288.1](https://doi.org/10.1175/JCLI-D-12-00288.1).
- Kanamitsu, M., W. Ebisuzaki, J. Woollen, S. K. Yang, J. J. Hnilo, M. Fiorino, and G. L. Potter, 2002: NCEP–DOE AMIP-II Reanalysis (R-2). *Bull. Amer. Meteor. Soc.*, **83**, 1631–1643, doi:[10.1175/BAMS-83-11-1631](https://doi.org/10.1175/BAMS-83-11-1631).
- Knutson, T. R., and S. Manabe, 1995: Time-mean response over the tropical Pacific to increased CO₂ in a coupled ocean–atmosphere model. *J. Climate*, **8**, 2181–2199, doi:[10.1175/1520-0442\(1995\)008<2181:TMROTT>2.0.CO;2](https://doi.org/10.1175/1520-0442(1995)008<2181:TMROTT>2.0.CO;2).
- Kosaka, Y., and S.-P. Xie, 2013: Recent global-warming hiatus tied to equatorial Pacific surface cooling. *Nature*, **501**, 403–407, doi:[10.1038/nature12534](https://doi.org/10.1038/nature12534).
- Lee, J.-Y., and B. Wang, 2014: Future change of global monsoon in the CMIP5. *Climate Dyn.*, **42**, 101–119, doi:[10.1007/s00382-012-1564-0](https://doi.org/10.1007/s00382-012-1564-0).
- , —, K.-H. Seo, J.-S. Kug, Y.-S. Choi, Y. Kosaka, and K.-J. Ha, 2014: Future change of Northern Hemisphere summer tropical–extratropical teleconnection in CMIP5 models. *J. Climate*, **27**, 3643–3664, doi:[10.1175/JCLI-D-13-00261.1](https://doi.org/10.1175/JCLI-D-13-00261.1).
- L’Heureux, M. L., S. Lee, and B. Lyon, 2013: Recent multidecadal strengthening of the Walker circulation across the tropical Pacific. *Nat. Climate Change*, **3**, 571–576, doi:[10.1038/nclimate1840](https://doi.org/10.1038/nclimate1840).
- Li, W., and Coauthors, 2013: Intensification of the Southern Hemisphere summertime subtropical anticyclones in a warming climate. *Geophys. Res. Lett.*, **40**, 5959–5964, doi:[10.1002/2013GL058124](https://doi.org/10.1002/2013GL058124).
- Lin, J.-L., 2007: The double-ITCZ problem in IPCC AR4 coupled GCMs: Ocean–atmosphere feedback analysis. *J. Climate*, **20**, 4497–4525, doi:[10.1175/JCLI4272.1](https://doi.org/10.1175/JCLI4272.1).
- Liu, Z., S. Vavrus, F. He, N. Wen, and Y. Zhong, 2005: Rethinking tropical ocean response to global warming: The enhanced equatorial warming. *J. Climate*, **18**, 4684–4700, doi:[10.1175/JCLI3579.1](https://doi.org/10.1175/JCLI3579.1).
- Lu, J., and B. Zhao, 2012: The role of oceanic feedback in the climate response to doubling CO₂. *J. Climate*, **25**, 7544–7563, doi:[10.1175/JCLI-D-11-00712.1](https://doi.org/10.1175/JCLI-D-11-00712.1).
- Ma, J., and S.-P. Xie, 2013: Regional patterns of sea surface temperature change: A source of uncertainty in future projections of precipitation and atmospheric circulation. *J. Climate*, **26**, 2482–2501, doi:[10.1175/JCLI-D-12-00283.1](https://doi.org/10.1175/JCLI-D-12-00283.1).
- , —, and Y. Kosaka, 2012: Mechanisms for tropical tropospheric circulation change in response to global warming. *J. Climate*, **25**, 2979–2994, doi:[10.1175/JCLI-D-11-00048.1](https://doi.org/10.1175/JCLI-D-11-00048.1).
- Meng, Q., M. Latif, W. Park, N. S. Keenlyside, V. A. Semenov, and T. Martin, 2012: Twentieth century Walker circulation change: Data analysis and model experiments. *Climate Dyn.*, **38**, 1757–1773, doi:[10.1007/s00382-011-1047-8](https://doi.org/10.1007/s00382-011-1047-8).
- Muller, C. J., and P. A. O’Gorman, 2011: An energetic perspective on the regional response of precipitation to climate change. *Nat. Climate Change*, **1**, 266–271, doi:[10.1038/nclimate1169](https://doi.org/10.1038/nclimate1169).
- Power, S. B., and G. Kociuba, 2011: What caused the observed twentieth-century weakening of the Walker circulation? *J. Climate*, **24**, 6501–6514, doi:[10.1175/2011JCLI4101.1](https://doi.org/10.1175/2011JCLI4101.1).
- Roeckner, E., and Coauthors, 1996: The atmospheric general circulation model ECHAM-4: Model description and simulation of present-day climate. MPI Rep. 218, 90 pp. [Available online at http://www.mpimet.mpg.de/fileadmin/publikationen/Reports/MPI-Report_218.pdf.]
- Sandeep, S., F. Stordal, P. D. Sardeshmukh, and G. P. Compo, 2014: Pacific Walker circulation variability in coupled and uncoupled climate models. *Climate Dyn.*, **43**, 103–117, doi:[10.1007/s00382-014-2135-3](https://doi.org/10.1007/s00382-014-2135-3).
- Solomon, A., and M. Newman, 2012: Reconciling disparate twentieth-century Indo-Pacific ocean temperature trends in the instrumental record. *Nat. Climate Change*, **2**, 691–699, doi:[10.1038/nclimate1591](https://doi.org/10.1038/nclimate1591).
- Sugi, M., and J. Yoshimura, 2004: A mechanism of tropical precipitation change due to CO₂ increase. *J. Climate*, **17**, 238–243, doi:[10.1175/1520-0442\(2004\)017<0238:AMOTPC>2.0.CO;2](https://doi.org/10.1175/1520-0442(2004)017<0238:AMOTPC>2.0.CO;2).
- Taylor, K. E., R. J. Stouffer, and G. A. Meehl, 2012: An overview of CMIP5 and the experiment design. *Bull. Amer. Meteor. Soc.*, **93**, 485–498, doi:[10.1175/BAMS-D-11-00094.1](https://doi.org/10.1175/BAMS-D-11-00094.1).
- Tokinaga, H., S.-P. Xie, C. Deser, Y. Kosaka, and Y. M. Okumura, 2012a: Slowdown of the Walker circulation driven by tropical Indo-Pacific warming. *Nature*, **491**, 439–443, doi:[10.1038/nature11576](https://doi.org/10.1038/nature11576).
- , —, A. Timmermann, S. McGregor, T. Ogata, H. Kubota, and Y. M. Okumura, 2012b: Regional patterns of tropical Indo-Pacific climate change: Evidence of the Walker circulation weakening. *J. Climate*, **25**, 1689–1710, doi:[10.1175/JCLI-D-11-00263.1](https://doi.org/10.1175/JCLI-D-11-00263.1).
- Vecchi, G. A., and B. J. Soden, 2007: Global warming and the weakening of the tropical circulation. *J. Climate*, **20**, 4316–4340, doi:[10.1175/JCLI4258.1](https://doi.org/10.1175/JCLI4258.1).
- , —, A. T. Wittenberg, I. M. Held, A. Leetmaa, and M. J. Harrison, 2006: Weakening of tropical Pacific atmospheric circulation due to anthropogenic forcing. *Nature*, **441**, 73–76, doi:[10.1038/nature04744](https://doi.org/10.1038/nature04744).
- , A. C. Clement, and B. J. Soden, 2008: Examining the tropical Pacific’s response to global warming. *Eos, Trans. Amer. Geophys. Union*, **89**, 81–83, doi:[10.1029/2008EO090002](https://doi.org/10.1029/2008EO090002).
- Xiang, B., and B. Wang, 2013: Mechanisms for the advanced Asian summer monsoon onset since the mid-to-late 1990s. *J. Climate*, **26**, 1993–2009, doi:[10.1175/JCLI-D-12-00445.1](https://doi.org/10.1175/JCLI-D-12-00445.1).

- , —, Q. Ding, F.-F. Jin, X. Fu, and H.-J. Kim, 2012: Reduction of the thermocline feedback associated with mean SST bias in ENSO simulation. *Climate Dyn.*, **39**, 1413–1430, doi:[10.1007/s00382-011-1164-4](https://doi.org/10.1007/s00382-011-1164-4).
- , —, A. Lauer, J.-Y. Lee, and Q. Ding, 2014: Upper tropospheric warming intensifies sea surface warming. *Climate Dyn.*, **43**, 259–270, doi:[10.1007/s00382-013-1928-0](https://doi.org/10.1007/s00382-013-1928-0).
- Xie, S.-P., C. Deser, G. A. Vecchi, J. Ma, H. Teng, and A. T. Wittenberg, 2010: Global warming pattern formation: Sea surface temperature and rainfall. *J. Climate*, **23**, 966–986, doi:[10.1175/2009JCLI3329.1](https://doi.org/10.1175/2009JCLI3329.1).
- , B. Lu, and B. Xiang, 2013: Similar spatial patterns of climate responses to aerosol and greenhouse gas change. *Nat. Geosci.*, **6**, 828–832, doi:[10.1038/ngeo1931](https://doi.org/10.1038/ngeo1931).
- Zhao, M., I. M. Held, S.-J. Lin, and G. A. Vecchi, 2009: Simulations of global hurricane climatology, interannual variability, and response to global warming using a 50-km resolution GCM. *J. Climate*, **22**, 6653–6678, doi:[10.1175/2009JCLI3049.1](https://doi.org/10.1175/2009JCLI3049.1).